Conference on Modelling Fluid Flow (CMFF'22)
The 18th International Conference on Fluid Flow Technologies
Budapest, Hungary, August 30 -September 2, 2022

HEAT TRANSFER AND FLUID FLOW ANALYSIS FOR ELECTROOSMOTIC FLOW OF CARREAU FLUID THROUGH A WAVY MICROCHANNEL CONSIDERING STERIC EFFECT

Sumit Kumar MEHTA[1], Sukumar PATI[2], László BARANYI[3]

[1]Department of Mechanical Engineering, National Institute of Technology Silchar, Silchar, India-788010, E-mail: sumit090391@gmail.com
[2] Corresponding Author: Department of Mechanical Engineering, National Institute of Technology Silchar, Silchar, India-788010, E-mail: sukumar@mech.nits.ac.in
[3] Department of Fluid and Heat Engineering, Institute of Energy Engineering and Chemical Machinery, University of Miskolc, 3515, Miskolc-Egyetemváros, Hungary. E-mail: laszlo.baranyi@uni-miskolc.hu

ABSTRACT

We investigate the heat transfer and flow characteristics for an electroosmotic flow of Carreau fluid through a wavy microchannel, considering the finite size of ions i.e., steric effect. The flow of electrolytic liquid is considered steady, two-dimensional and incompressible. The modified Poisson-Boltzmann equation, Laplace equation, continuity equation, momentum equation, and energy equation are solved numerically using a finite element method-based solver. The computed flow and temperature fields are validated by comparison with published results. The flow and temperature fields and average Nusselt number are computed by varying the steric factor, Weissenberg number and Brinkman number in the following ranges: $0 \leq \upsilon \leq 0.3$, $0.01 \leq Wi \leq 1$, $10^{-5} \leq Br \leq 10^{-3}$. We found the locations of the local maxima and minima of Nusselt number at the convex and concave surfaces of the channel for a lower Brinkman number ($=10^{-5}$). In contrast, the corresponding locations are swapped at higher Brinkman number ($=10^{-3}$). The value of average Nusselt number increases with the increase in Weissenberg number and decreases with the steric factor for the smaller Brinkman number ($=10^{-5}$). Whereas, it decreases with Wi for non-zero values the of steric factor with higher Brinkman number ($=10^{-3}$).

Keywords: Electroosmosis; heat transfer; steric effect; viscous heating, wavy microchannel.

NOMENCLATURE

Br	[-]	Brinkman number
E^*_{ref}	[V/m]	Reference external electric field
G	[-]	Joule heating parameter
H	[m]	Inlet half height of microchannel
Nu	[-]	Nusselt number
$\overline{Nu}$	[-]	Average Nusselt number
q	[W/m^2]	Heat flux
$\mathbf{u}$	[-]	Dimensionless velocity vector
Wi	[-]	Weissenberg number
υ	[-]	Steric factor

1. INTRODUCTION

In recent times, analysis of transport phenomena in microfluidic channels has received serious attention due to its wide range of engineering applications, such as biomedical and pharmaceutical industries. For microfluidic transport of electrolyte, flow actuated by an external electrical forcing also known as electroosmotic flow (EOF) is one of the suitable flow actuation mechanism widely used due to better flow control and simplicity of the system [1-8]. Further, the micro-level heat exchanging systems using EOF is getting significant attention because of its applications in electronics cooling [9].

Using wavy surfaces, the fluid-solid interfacial area for heat transfer can be enhanced and accordingly channel with wavy walls wall is one of the effective methods for heat transfer enhancement [10-15]. Cho et al. [16] investigated the heat transfer characteristics for the combined electroosmotic and pressure-driven flow through a complex wavy microchannel considering the Joule heating effect. They found that the value of maxima of Nusselt number increases with the increase in the amplitude of the complex wavy wall.

For several microfluidic applications, fluid is non-Newtonian in nature [3]. Researchers have developed and employed several models, namely, power-law model [17], Carreau model [3], Casson model [18], moldflow second-order model [19] to describe the constitutive behaviour of non-Newtonian fluids. Moghadam [20] investigated the heat transfer characteristics for electrokinetic-driven flow of non-Newtonian power-law fluid through a circular microtube and found that the trend of fully developed Nusselt number is either increasing or decreasing with the increase in flow behaviour index and the length scale ratio. Noreen et al. [21] studied the heat transfer characteristics for electroosmotic flow of Carreau fluid through a wavy microchannel and reported that the increase in Weissenberg number increases the Nusselt number.

The classical Poisson-Boltzmann model over-predicts the ionic concentration in electric double-layer (EDL) by neglecting the effect of finite ion size. However, the effect of ions size cannot be ignored for the higher surface charge density. Accordingly, several researchers have used the modified Poisson-Boltzmann equation duly incorporating the effect of finite size of ions by introducing steric factor to find the EDL potential [22, 23]. Dey et al. [24] investigated the effect of finite size of ions on the heat transfer characteristics for combined electroosmotic and pressure-driven flow through the microchannel. They reported that the point charge assumption overestimates the Nusselt number.

This brief literature survey reveals that no work has been reported investigating the effect of finite size of ions on the heat transfer characteristics for flow of Carreau fluid in a wavy microchannel, which is the main focus of the present work.

2. THEORETICAL FORMULATION

We consider an electroosmotic flow of Carreau fluid through a wavy microchannel with inlet half-height, $2H$, as shown in Fig. 1. Both walls of the channel at the inlet and outlet are planar having an axial length of $5H$ each and in the intermediate part having an axial length of $20H$, the walls are wavy, the sinusoidal profiles of which are taken as [3, 8, 16]:

$$S^*_{Top}\left(x^*\right) = 2H + 0.3H\sin\left(\pi\left(x^* - 5H\right)/H\right) \tag{1}$$

$$S^*_{Bottom}\left(x^*\right) = 0.3H\sin\left(\pi\left(x^* - 5H\right)/H\right). \tag{2}$$

The amplitude of the wavy walls is taken as 0.3 times of the inlet half-height [3, 8, 16], such that the curvature effect on the ionic distribution can be neglected as the radius of curvature ($\left(H_w/4\right)^2/A = 5.2H \gg H$) is large compared to the inlet half-height [3], where, $H_w\left(=5H\right)$ is the wavelength. The planar walls are insulated, while the wavy walls are imposed with constant heat flux q. It is assumed that flow of electrolytic liquid is steady, two-dimensional and incompressible. The temperature-independent thermo-physical properties are taken into consideration. Moreover, the ionic distribution is static as the ionic Peclet number is smaller than unity. The governing equations (modified Poisson-Boltzmann equation, Laplace equation, continuity equation, momentum equation and energy equation) in dimensionless form relevant to the present work are as follows [3, 21]:

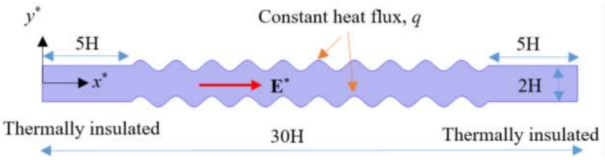

Figure 1. Physical domain.

$$\nabla^2\psi = \kappa^2 \frac{\sinh\left(\psi\right)}{1+4\upsilon\sinh^2\left(\psi/2\right)}, \tag{3}$$

$$\nabla^2\varphi = 0, \tag{4}$$

$$\nabla\cdot\mathbf{u} = 0, \tag{5}$$

$$Re\left(\mathbf{u}\cdot\nabla\right)\mathbf{u} = -\nabla P + \left(\nabla\cdot\boldsymbol{\tau}\right) + \left[\kappa^2\frac{\sinh\left(\psi\right)}{1+4\upsilon\sinh^2\left(\psi/2\right)}\right]\nabla\left(\psi/\Lambda+\varphi\right) \tag{6}$$

$$Pe\left(\mathbf{u}\cdot\nabla\theta\right) = \nabla^2\theta + Br\phi + G. \tag{7}$$

Here ψ and φ are the dimensionless induced and external potential fields normalized by the scale $\psi^*_{ref}\left(=k_BT/ze\right)$ and $\varphi^*_{ref}\left(=\Delta V\times H/30H\right)$, respectively; $\mathbf{u}\equiv\left(u,v\right)$ is the dimensionless velocity vector normalized by the Helmholtz-Smoluchowski velocity $u^*_{HS}\left(=-\psi^*_{ref}E^*_{ref}\varepsilon/\mu_o\right)$; $\nabla\equiv\left(\mathrm{x},\mathrm{y}\right)$ is normalized by H; pressure P is normalised by $\mu_o u^*_{HS}/H$; $\boldsymbol{\tau} = \boldsymbol{\tau}^*\left(\mu_o u^*_{HS}/H\right)^{-1}$ is the dimensionless deviatoric stress tensor, where $\boldsymbol{\tau}^* = \mu\left(\dot{\gamma}^*\right)\left[\left(\nabla\mathbf{u}^*\right)+\left(\nabla\mathbf{u}^*\right)^T\right]$; $\dot{\gamma}^* = \sqrt{(1/2)(\mathbf{S}:\mathbf{S})}$ is the second invariant of the rate of deformation tensor and $\mathbf{S} = \left[\left(\nabla\mathbf{u}^*\right)+\left(\nabla\mathbf{u}^*\right)^T\right]$ is the strain rate tensor. The apparent viscosity for Carreau fluid can be written as [3]: $\mu\left(\dot{\gamma}^*\right) = \mu_\infty + \left(\mu_o-\mu_\infty\right)\left(1+\left(\lambda\dot{\gamma}^*\right)\right)^{((n-1)/2)}$,

where μ_∞, μ_o, λ, and n are the infinity and zero shear rate viscosity, relaxation time parameter, and flow behaviour index, respectively. Moreover, the dimensionless temperature is expressed as $\theta = \left(T-T_{in}\right)/\left(qH/k\right)$.

Here, $\phi = \left[\frac{\partial u}{\partial x}\left(\tau_{xx}-\tau_{yy}\right)+\left(\frac{\partial u}{\partial y}+\frac{\partial v}{\partial x}\right)\tau_{xy}\right]$ is the viscous dissipation parameter; $\tau_{xx} = 2\left(\bar{\mu}_\infty+\left(1-\bar{\mu}_\infty\right)\left(1+\left(\mathrm{Wi}\,\dot{\gamma}\right)\right)^{((n-1)/2)}\right)\frac{\partial u}{\partial x}$; $\tau_{xy} = \left(\bar{\mu}_\infty+\left(1-\bar{\mu}_\infty\right)\left(1+\left(\mathrm{Wi}\,\dot{\gamma}\right)\right)^{((n-1)/2)}\right)\left(\frac{\partial u}{\partial y}+\frac{\partial v}{\partial x}\right)$ and $\tau_{yy} = 2\left(\bar{\mu}_\infty+\left(1-\bar{\mu}_\infty\right)\left(1+\left(\mathrm{Wi}\,\dot{\gamma}\right)\right)^{((n-1)/2)}\right)\left(\frac{\partial v}{\partial y}\right)$ are the components of stresses, where $\dot{\gamma} = \sqrt{2\left(\frac{\partial u}{\partial x}\right)^2+\left(\frac{\partial u}{\partial y}+\frac{\partial v}{\partial x}\right)^2+2\left(\frac{\partial v}{\partial y}\right)^2}$ [21]. Here, $\bar{\mu}_\infty$ is defined as $\bar{\mu}_\infty = \mu_\infty/\mu_o$ the value of which is taken as 0.0616 [3]. Here, υ, $\kappa(=H/\lambda_D)$ and $Re\left(=\rho u_{HS}^* H/\mu_o\right)$ are the steric factor, Debye parameter, Reynolds number, respectively; $Wi=\left(\lambda u_{HS}^*/H\right)$, $\Lambda\left(=\varphi_{ref}^*/\psi_{ref}^*\right)$, and $Pe\left(=\rho c_p H u_{HS}^*/k\right)$ are the Weissenberg number, ratio of reference applied to EDL potential, thermal Peclet number, respectively; $Br\left(=\mu_o\left(u_{HS}^*/H\right)^2 H/q\right)$, and $G\left(=\sigma\left(E_{ref}^*\right)^2 H/q\right)$ are the Brinkman number, and Joule heating parameter, respectively. Note that $\lambda_D\left(=\left(2n_o z^2 e^2/\varepsilon k_B T\right)^{-0.5}\right)$, ΔV, ρ, c_p, k, ε, $E_{ref}^*\left(=\Delta V/30H\right)$, n_o, T and σ are the Debye length, applied external potential difference, density, specific heat capacity, thermal conductivity, electrical permittivity of the liquid, reference external electric field, bulk ionic concentration, reference absolute temperature, and electrical conductivity of the liquid, respectively.

The boundary conditions employed are follows:

At inlet:

$$\mathbf{n}\cdot(\nabla\psi)=0,\ \varphi=30,\ P=P_{atm},\ \theta=0. \tag{8a}$$

At wavy walls:

$$\psi=\zeta=4,\ \mathbf{n}\cdot(\nabla\varphi)=0,\ \mathbf{u}=0,\ \partial\theta/\partial n=1. \tag{8b}$$

At planar walls:

$$\psi=4,\ \mathbf{n}\cdot(\nabla\varphi)=0,\ \mathbf{u}=0,\ \partial\theta/\partial n=0 \quad . \tag{8c}$$

At outlet:

$$\mathbf{n}\cdot(\nabla\psi)=0,\ \varphi=0,\ P=P_{atm},\ \partial\theta/\partial x=0. \tag{8d}$$

Here $\mathbf{n}$ is the unit vector normal to wavy wall.

The heat transfer rate is presented in terms of local Nusselt number (Nu) as [1, 7]:

$$Nu=1/\left(\theta_{wall}-\theta_{mean}\right) \tag{9}$$

Here $\theta_{mean}\left(=\int_{y_1}^{y_2} u\theta \,\mathrm{d}y \Big/ \int_{y_1}^{y_2} u \,\mathrm{d}y\right)$ is the bulk mean temperature of the fluid [7].

The average Nusselt number $\left(\overline{Nu}\right)$ is calculated as [11, 12, 14]:

$$\overline{Nu}=0.5\left[\left(\int_{x=5}^{x=25} Nu\,\mathrm{d}S \Big/ \int_{x=5}^{x=25}\mathrm{d}S\right)_{Top}+\left(\int_{x=5}^{x=25} Nu\,\mathrm{d}S \Big/ \int_{x=5}^{x=25}\mathrm{d}S\right)_{Bottom}\right] \tag{10}$$

Here S is the normalised axial length of the wavy walls.

3. NUMERICAL METHODOLOGY AND MODEL BENCHMARKING

We employ a finite element method based numerical solver to obtain the flow and temperature fields. The computational domain is divided into large number of small sub-domains in non-uniform manner with denser mesh near the walls. The mesh used for the present computational investigation is presented in Fig. 2. Using Galerkin weighted method, the governing equations are first discretised and then the resulting equations are solved iteratively until the pre-defined residual value of 10^{-6} is reached. An exhaustive grid independence test was performed by calculating the average Nusselt number as depicted in Table 1; the relative difference of the value for the mesh system with 130144 elements and the next level finer mesh was less than 1%. Accordingly, the mesh with 130144 elements was used for all the simulations.

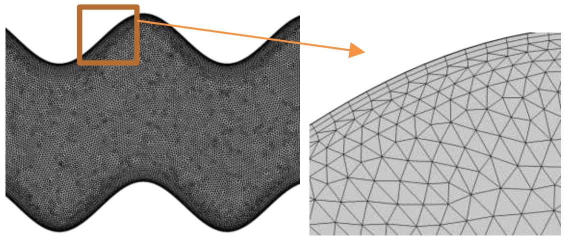

Figure 2. Grid distribution in wavy microchannel.

Table 1. Grid independence test at different mesh system (M) calculating average Nusselt number when υ =0.3, n=0.4, Wi=1, Br=10^{-3} and κ=30.

Mesh type	Number of elements	Average Nusselt number	Percentage error w r t M4
M1	20206	3.5294	24.586
M2	51869	3.0219	6.671
M3	130144	2.8376	0.166
M4	218108	2.8329	0

We validate the solver by comparing the electroosmotic flow velocity profile with the results of Zhao et al. [5] for parallel plate channel shown in Fig. 3(a) for n=1, κ=10, υ=0 and ζ=1. The second validation is presented in Fig. 3(b) by comparing the dimensionless wall temperature for EOF in a plane microchannel with the results of Horiuchi and Dutta [25]. For this validation, the values of different parameters considered are as follows: Pe=100, κ=100, Br=0, n=1 and υ=0. The comparisons show a good agreement of the present result with the published works [5, 25].

4. RESULTS AND DISCUSSION

We analyse the heat transfer and flow characteristics for an ionic size dependent electroosmotic flow of Carreau fluid through a wavy microchannel. The results are presented in terms of flow and temperature fields, local Nusselt number (Nu) and average Nusselt number ($\overline{Nu}$) by varying the steric factor (υ), Weissenberg number (Wi) and Brinkman number (Br) in the range of 0≤ υ ≤0.3, 0.01≤Wi ≤1, [3, 21, 26], and 10^{-5}≤ Br ≤10^{-3}, respectively [1, 5]. The value of n and Re is kept fixed at 0.4 and 0.001, respectively [3, 26].

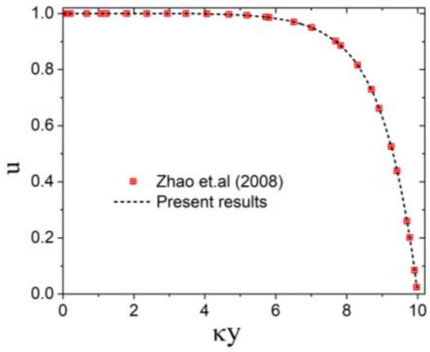

(a)

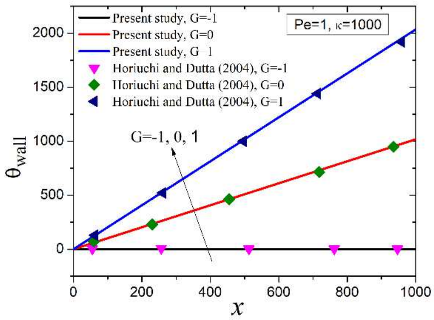

(b)

Figure 3. (a) Comparison of dimensionless electroosmotic flow velocity in a parallel plate channel *κ*=10, *υ*=0 and *ζ*=1 at the limiting case, *n*=1, (b) Comparison of non-dimensional wall temperature for EOF through a plane microchannel for different *G* values with the results of Horiuchi and Dutta [25] for *Pe*=100, *κ*=100, *Br*=0, *n*=1 and *υ*=0.

Figure 4 shows the transverse variation of dimensionless flow velocity at *x*=10.5 for different values of *Wi* and *υ*. It is observed that the increase in *υ* from 0 to 0.3 decreases the flow velocity due to the increase in flow resistance caused by the electrostatic pull inside the EDL by the finite size of ions [3]. It is also seen that the decrement is higher near the walls as the flow resistance is only within the EDL. Furthermore, the flow velocity at any transverse location increases as *Wi* increases which is attributed to the decreases in apparent viscosity of the fluid.

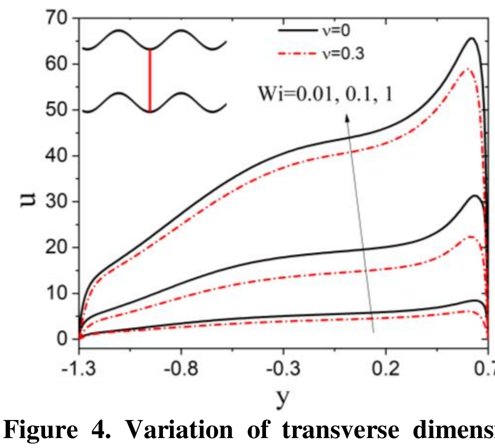

Figure 4. Variation of transverse dimensionless velocity profile at *x*=10.5 for different values of steric factor and *Wi*.

The streamlines and dimensionless flow velocity contours at different *Wi* are presented in Fig. 5 at *υ*=0.3. It is observed that the streamlines near the wall follow the profile of the wavy walls and accordingly they become a wavy. Further, the minima and maxima of velocity exist near the concave and convex surfaces due to the smaller and higher electric field intensity, respectively. Moreover, the flow velocity is enhanced with *Wi* due to the decrease in the apparent viscosity of the fluid.

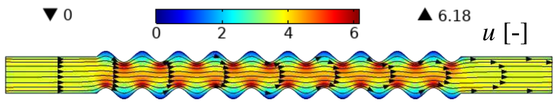

(a) *Wi*=0.01

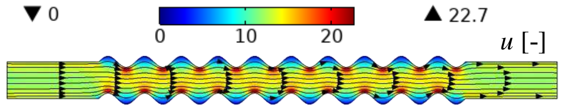

(b) *Wi*=0.1

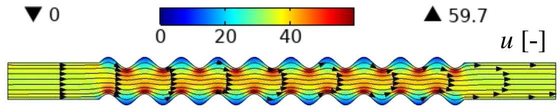

(c) *Wi*=1

Figure 5. Streamlines and dimensionless flow velocity contours at different *Wi* for *υ* =0.3, *n*=0.4 and *κ*=30.

Figures 6(a) and (b) show the contours of dimensionless isotherms at different *Wi* and *Br* for *υ*=0 and 0.3, respectively. It is seen that the increase in *Wi* from 0.01 to 1 decreases the temperature in the domain due to the increase in convective heat transfer (see Fig. 4). Further, the decrease in convection strength with the increase in steric factor from 0 to 0.3 (see Fig. 4) increases the isotherms values for *υ*=0.3 compared to *υ*=0. It is also noted that the increase in *Br* augments the temperature of fluid due to the increase in viscous dissipation effect. The increment is significantly higher for the higher *Wi* (=1) values, which is attributed to the higher velocity gradient (see Fig. 4).

Figure 7(a) and (b) shows the variation of local Nusselt number (*Nu*) at the top wall for different *υ* values with $Br=10^{-5}$ and 10^{-3} at *Wi*=1. It is observed that the locations of the local maxima and minima of *Nu* are at the convex and concave surfaces, respectively due to higher and smaller velocity gradient for the smaller *Br* ($=10^{-5}$). In contrast, these minima and maxima locations are shifted to convex and concave surface, respectively at $Br=10^{-3}$. It is attributed to the higher velocity near the convex surface causing very high viscous dissipation effect at higher *Br*. Furthermore, the increase in υ decreases the value of *Nu* for $Br=10^{-5}$ and the trend is opposite for $Br=10^{-3}$. These observations can be explained as follows. For smaller *Br* ($=10^{-5}$) values the significant increase in wall temperature compared to the core temperature (see Fig. 6) due to the decrease in flow velocity (see Fig. 4) increases the difference of (θ_{wall}

- θ_{mean}) with υ. Whereas, for higher Br (=10^{-3}), the decrease in velocity gradient with υ (see Fig. 4) near the walls significantly reduces the viscous heating and augments the heat transfer rate with υ.

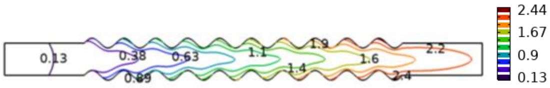

Br=10^{-5}, Wi=0.01

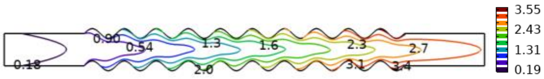

Br=10^{-3}, Wi=0.01

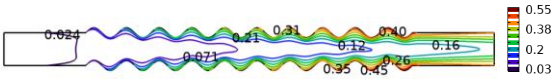

Br=10^{-5}, Wi=1

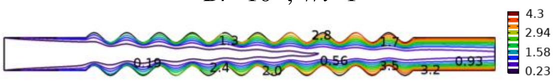

Br=10^{-3}, Wi=1

(a) υ=0

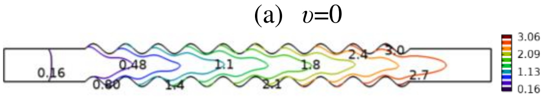

Br=10^{-5}, Wi=0.01

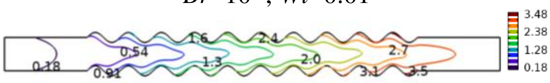

Br=10^{-3}, Wi=0.01

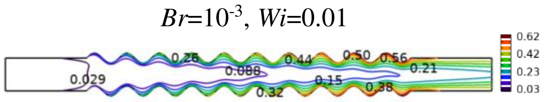

Br=10^{-5}, Wi=1

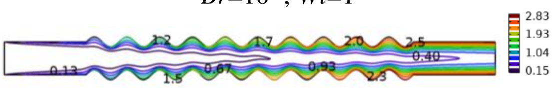

Br=10^{-3}, Wi=1

(b) υ=0.3

Figure 6. Contours of dimensionless isotherms for different *Br* and *Wi* values at (a) υ=0 and (b) υ=0.3, when ζ=4, κ=30, *Pe*=5, *n*=0.4 and *G*=1. The colour legends represent the dimensionless temperature, θ.

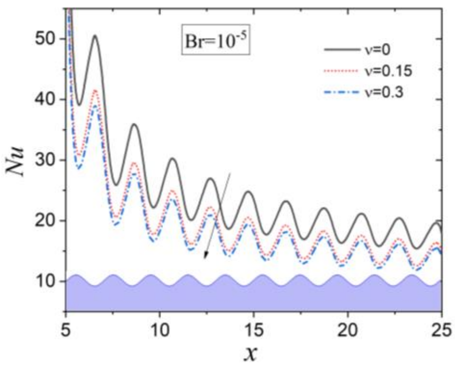

(a)

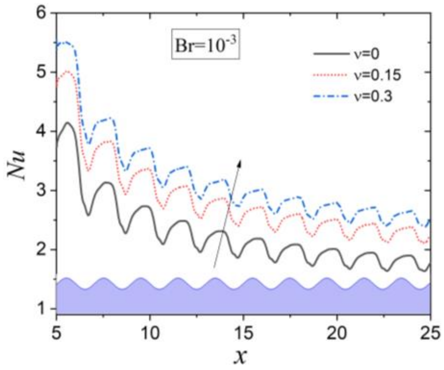

(b)

Figure 7. Variation of local Nusselt number at different υ values for (a) Br=10^{-5} and (b) Br=10^{-3} when ζ=4, κ=30, *Pe*=5, *n*=0.4 and *G*=1.

The variation of average Nusselt number ($\overline{Nu}$) with *Wi* for different υ values is shown in Fig. 8(a) and (b) for Br=10^{-5} and 10^{-3}, respectively. It is

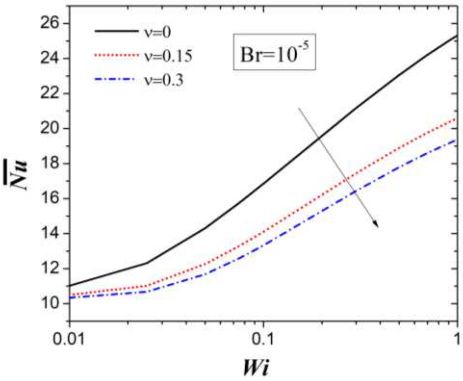

(a)

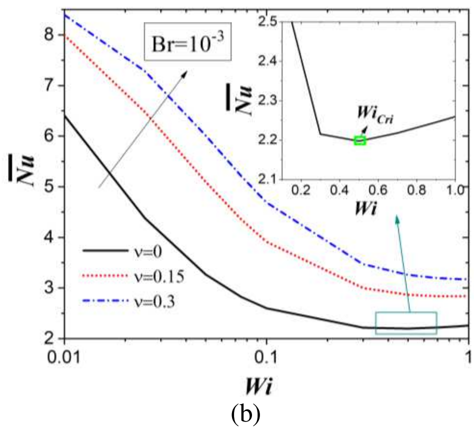

(b)

Figure 8. Variation of average Nusselt number with *Wi* at different υ values for (a) Br=10^{-5} and (b) Br=10^{-3} when ζ=4, κ=30, *Pe*=5, *n*=0.4 and *G*=1.

observed that the value of $\overline{Nu}$ increases with *Wi* for Br =10^{-5}. It is attributed to fact that the increase in flow velocity with *Wi* (see Fig. 4) significantly reduces the wall temperature compared to the bulk temperature and the decrease in (θ_{wall} - θ_{mean}) with *Wi* increases the value of $\overline{Nu}$. Also, it is seen in Fig. 8(a) that $\overline{Nu}$ decreases with υ for smaller (Br =10^{-5})

which can be explained from the variation of local Nusselt number with υ. The value of $\overline{Nu}$ decreases with Wi for υ=0.15 and 0.3, and it follows the increasing-decreasing trend with Wi for the point charge case (υ=0), and a critical Wi (Wi_{Cri}) is found for Br=10^{-3}. The decrease in $\overline{Nu}$ with Wi is attributed to the augmentation in viscous heating (see Fig. 4), which decreases the heat transfer rate. Whereas, for higher Wi values (>Wi_{Cri}), the enhanced convective strength decreases the core region temperature and hence the value of (θ_{wall} - θ_{mean}). Furthermore, it is seen in Fig. 8(b) that the value of $\overline{Nu}$ increases with υ which can be explained from the variation of local Nusselt number. The values of the decrease and increase in $\overline{Nu}$ are obtained as 23.49% and 40.51% for change in υ from 0 to 0.3 for Br=10^{-5} and 10^{-3}, respectively, when Wi=1.

5. CONCLUSIONS

In the present study we investigate the heat transfer and flow characteristics for an ionic size dependent electroosmotic flow of non-Newtonian Carreau fluid through a wavy microchannel. The results are presented in terms of flow and temperature fields, local Nusselt number (Nu) and average Nusselt number ($\overline{Nu}$) by varying the steric factor (υ), Weissenberg number (Wi) and Brinkman number (Br) in the following range: $0\leq \upsilon \leq 0.3$, $0.01\leq Wi \leq 1$, [3, 21, 26], and $10^{-5}\leq Br \leq 10^{-3}$. The important findings are summarised as follows:

- The flow velocity increases with Wi and decreases with υ.
- The locations of the local maxima and minima of Nusselt number are at the convex and concave surfaces for smaller Br (=10^{-5}). In contrast, the locations are swapped at higher Br (=10^{-3}).
- The value of $\overline{Nu}$ increases with Wi and decreases with υ for smaller Br (=10^{-5}) values. Whereas the value of $\overline{Nu}$ decreases with Wi for υ=0.15 and 0.3, and it follows the increasing-decreasing trend with Wi for point charge case (υ=0), and a critical Wi is found for higher Br (=10^{-3}). Moreover, $\overline{Nu}$ increases with υ for higher Br (=10^{-3}).
- The values of the decrease and increase in $\overline{Nu}$ are obtained as 23.49% and 40.51% for the change in υ from 0 to 0.3 for Br=10^{-5} and Br=10^{-3}, respectively, when Wi=1.

REFERENCES

[1] Pabi, S., Mehta, S.K., and Pati S., 2021, “Analysis of thermal transport and entropy generation characteristics for electroosmotic flow through a hydrophobic microchannel considering viscoelectric effect”, *Int Commun Heat Mass Transf*, Vol. 127, p. 105519.

[2] Vasista, K.N., Mehta, S.K., Pati, S., and Sarkar, S., 2021, “Electroosmotic flow of viscoelastic fluid through a microchannel with slip-dependent zeta potential”, *Phys Fluids*, Vol. 33, p. 123110.

[3] Mehta, S.K., Pati, S., and Mondal, P.K., 2021, “Numerical study of the vortex-induced electroosmotic mixing of non-Newtonian biofluids in a nonuniformly charged wavy microchannel: Effect of finite ion size”. *Electrophoresis*, Vol. 42, pp. 2498-2510.

[4] Sujith T., Mehta, S.K., and Pati, S., 2021, “Effect of non-uniform heating on electroosmotic flow through microchannel”, *Recent Advances in Mechanical Engineering. In: Pandey KM, Misra RD, Patowari PK, Dixit US, editors. Springer Singapore*; pp. 499–508. https://doi.org/10.1007/978-981-15-7711-6_50

[5] Zhao, C., Zhao, E., Masliyah, J.H., and Yang, C., 2008, “Analysis of electroosmotic flow of power-law fluids in a slit microchannel”, *J. Colloid Interface Sci.* Vol. 326, pp. 503–510.

[6] Mondal, B., Mehta, S.K., Pati, S., and Patowari, P.K., 2021, “Numerical analysis of electroosmotic mixing in a heterogeneous charged micromixer with obstacles” *Chem Eng Process - Process Intensif*. Vol. 168, p. 108585.

[7] Banerjee, D., Mehta, S.K., Pati, S., and Biswas, P., 2021, “Analytical solution to heat transfer for mixed electroosmotic and pressure-driven flow through a microchannel with slip-dependent zeta potential”, Int *J Heat Mass Transf*. Vol. 181, p. 121989.

[8] Vasista, K.N., Mehta, S.K., and Pati, S., 2021, “Numerical assessment of hydrodynamic and mixing characteristics for mixed electroosmotic and pressure-driven flow through a wavy microchannel with patchwise surface heterogeneity”, *Proc Inst Mech Eng Part E J Process Mech Eng*. https://doi.org/10.1177/09544089211051640

[9] Eng, P.F., Nithiarasu, P., Arnold, A.K., Igic, P., and Guy, O. J.,2007, “Electro-osmotic flow based cooling system for microprocessors”, *International Conference on Thermal, Mechanical and Multi-Physics Simulation Experiments in Microelectronics and Micro-Systems. EuroSime 2007*, pp. 1-5, https://doi.org/10.1109/ESIME.2007.360041

[10] Mehta, S.K., and Pati, S., 2019, “Analysis of thermo-hydraulic performance and entropy generation characteristics for laminar flow through triangular corrugated channel”, *J Therm Anal Calorim*. Vol. 136, pp. 49–62.

[11] Mehta, S.K., and Pati, S., 2021, “Thermo-hydraulic and entropy generation analysis for magnetohydrodynamic pressure driven flow of

nanofluid through an asymmetric wavy channel", *Int J Numer Methods Heat Fluid Flow*. Vol. 31, pp. 1190–213.

[12] Mehta, S.K., Pati, S., Ahmed S, Bhattacharyya, P., and Bordoloi, J.J., 2021, "Analysis of thermo-hydraulic and entropy generation characteristics for flow through ribbed-wavy channel", *Int J Numer Methods Heat Fluid Flow*. Vol. 32 No. 5, pp. 1618-1642.

[13] Pati, S., Mehta, S.K., and Borah, A., 2017, "Numerical investigation of thermo-hydraulic transport characteristics in wavy channels: Comparison between raccoon and serpentine channels", *Int Commun Heat Mass Transf*. Vol. 88, pp. 171–176.

[14] Mehta, S.K., Pati, S., and Baranyi, L., 2022, "Effect of amplitude of walls on thermal and hydrodynamic characteristics of laminar flow through an asymmetric wavy channel", *Case Stud Therm Eng*. Vol. 31, p. 101796.

[15] Mehta, S.K., and Pati, S., 2020, "Numerical study of thermo-hydraulic characteristics for forced convective flow through wavy channel at different Prandtl numbers", *J Therm Anal Calorim*. Vol. 141, pp. 2429–2451.

[16] Cho, C.C., Chen, C.L., and Chen, C.K., 2012, "Characteristics of combined electroosmotic flow and pressure-driven flow in microchannels with complex-wavy surfaces", *Int J Therm Sci.* Vol. 61, pp. 94–105.

[17] Babaie, A., Sadeghi, A., and Saidi, M.H., 2011, "Combined electroosmotically and pressure driven flow of power-law fluids in a slit microchannel", *J Nonnewton Fluid Mech*. Vol. 166, pp. 792–798.

[18] Bag, N., and Bhattacharyya, S., 2018, "Electroosmotic flow of a non-Newtonian fluid in a microchannel with heterogeneous surface potential", *J Nonnewton Fluid Mech*. Vol. 259, pp. 48–60.

[19] Koh, Y.H., Ong, N.S., Chen, X.Y., Lam, Y.C., and Chai, J.C., 2004, "Effect of temperature and inlet velocity on the flow of a nonnewtonian fluid", *Int Commun Heat Mass Transf.* Vol. 31, pp. 1005–1013.

[20] Moghadam, A.J., 2013, "Electrokinetic-driven flow and heat transfer of a non-Newtonian fluid in a circular microchannel". *J Heat Transfer*. Vol. 135, p. 021705.

[21] Noreen, S, Waheed S., Hussanan, A., and Lu, D., 2019, "Analytical solution for heat transfer in electroosmotic flow of a Carreau fluid in a wavy microchannel", *Appl Sci.*, Vol. 9(20), p. 4359.

[22] Liu, Y., and Jian, Y., 2019, "The effects of finite ionic sizes and wall slip on entropy generation in electroosmotic flows in a soft nanochannel". *J Heat Transfer*. Vol. 141. p. 102401.

[23] Fadaei, P., Niazmand, H., and Raoufi, M.A., 2022, "Influence of finite size of ions on thermal transport of a simultaneous electrokinetic-pressure driven flow of power-law fluids in a slit microchannel", *Colloids Surfaces A Physicochem Eng Asp.* Vol. 634, p. 127857.

[24] Dey, R., Ghonge, T., and Chakraborty, S., 2013, "Steric-effect-induced alteration of thermal transport phenomenon for mixed electroosmotic and pressure driven flows through narrow confinements", *Int J Heat Mass Transf.* Vol. 56, pp. 251–262.

[25] Horiuchi, K., and Dutta, P., 2004, "Joule heating effects in electroosmotically driven microchannel flows" *Int J Heat Mass Transf.* Vol. 47, pp. 3085–3095.

[26] Hayat, T., Saleem, N., and Ali, N., 2010, "Effect of induced magnetic field on peristaltic transport of a Carreau fluid", *Commun Nonlinear Sci Numer Simul.*, Vol. 15, pp. 2407–2423.